Bone morphogenetic protein 4 inhibits insulin secretion from rodent beta cells through regulation of calbindin1 expression and reduced voltage-dependent calcium currents

Christensen, Gitte L.; Jacobsen, Maria L. B.; Wendt, Anna; Mollet, Ines; Friberg, Josefine; Frederiksen, Klaus S.; Meyer, Michael; Bruun, Christine; Eliasson, Lena; Billestrup, Nils

Published in:
Diabetologia

DOI:
10.1007/s00125-015-3568-x

2015

Bone Morphogenetic Protein 4 inhibits insulin secretion from rodent beta cells through regulation of Calbindin1 expression and reduced voltage dependent calcium currents.

Authors: Gitte L. Christensen[1], Maria L. B. Jacobsen[1], Anna Wendt[2], Ines G. Mollet[2], Josefine Friberg[1], Klaus S. Frederiksen[3], Michael Meyer[4], Christine Bruun[5], Lena Eliasson[2$] and Nils Billestrup[1$]

(1) Department of Biomedical Sciences, University of Copenhagen, Copenhagen, Denmark, (2) Lund University Diabetes Center, Lund University, Malmø, Sweden, (3) Biopharmaceuticals Research Unit, Novo Nordisk A/S, Måløv, Denmark, (4) Department of Cellular Physiology, Ludwig-Maximilians-Universität, Munich, (5) Department of Incretin and Islet Biology, Novo Nordisk A/S, Måløv, Denmark.

[$] Corresponding authors: Lena Eliasson, Lund University Diabetes Center, Lund University, Malmø, Sweden, Lena.Eliasson@med.lu.se, +46-40391153 and Nils Billestrup, Department of Biomedical Sciences, University of Copenhagen, Nørre Alle 20, DK-2100 Copenhagen, Billestrup@sund.ku.dk, phone: +45-29607952.

Running title: Mechanisms in BMP4 inhibition of insulin secretion

Keywords: Diabetes, beta cells , insulin secretion, exocytosis, BMP4, Calbindin1

Word count: Abstract: 237 Main text: 3999 Figures: 4 Tables: 1

Online only supplementary information: 2 Tables, 2 Figures

Abbreviations:

BMP: Bone Morphogenetic protein

CDF: Chip definition file

ECM: Extracellular matrix

FDR: False discovery rate

GSIS: Glucose stimulated insulin secretion

HBSS: Hanks' balanced salt solution

Id1: Inhibitor of differentiation 1

Ins1: Insulin 1

KO: Knock out

KRHB: Krebs Ringer Hepes Buffer

NCS: Newborn calf serum

TGF-β: Transforming Growth Factor-β

VDCC: Voltage dependent calcium channel

WT: Wild type

Abstract

Aims/hypothesis: Type 2 diabetes is characterized by progressive loss of pancreatic beta cell mass and function. Therefore, it is of therapeutic interest to identify factors with potential to improve beta cell proliferation and insulin secretion. Bone morphogenetic protein 4 (BMP4) expression is increased in diabetic animals and BMP4 reduce glucose-stimulated insulin secretion (GSIS). Here we investigate the molecular mechanism behind this inhibition.

Methods: The BMP4 mediated inhibition of GSIS was investigated in detail using single cell electrophysiological measurements and live calcium imaging. BMP4 mediated gene expression changes were investigated with microarray profiling, q-pcr and western blotting.

Results: Prolonged exposure to BMP4 reduced GSIS from rodent pancreatic islets. This inhibition was associated with decreased exocytosis due to a reduced Ca^{2+}-current through voltage-dependent Ca^{2+}-channels. To identify proteins involved in the observed inhibition of GSIS we investigated the global gene expression changes induced by BMP4 in neonatal rat pancreatic islets. The expression of the Ca^{2+}-binding protein Calbindin1 was induced significantly by BMP4. Overexpression of Calbindin1 in primary islet cells reduced GSIS and the effect of BMP4 on GSIS was lost in islets from Calbindin1 knock out mice.

Conclusions/interpretation: We find BMP4 treatment to markedly inhibit GSIS from rodent pancreatic islets in a Calbindin1-dependent manner. Calbindin1 is suggested to mediate the effect of BMP4 by buffering Ca^{2+} and decreasing Ca^{2+}-channel activity resulting in diminished insulin exocytosis. BMP4 and Calbindin1 are both potential pharmacological targets for the treatment of beta cell dysfunction.

In response to insulin resistance, the pancreatic beta cells will initially compensate by increasing mass and function to maintain normal blood glucose levels [1]. In individuals who progress to develop type 2 diabetes the beta cells eventually fail to adapt and progressive loss of functional beta cells starts [1]. Although current type 2 diabetes drugs targeting insulin resistance or insulin secretion are initially efficient, beta cell mass and function tends to decline over time [2, 3]. Unidentified factors may limit the ability of the beta cells to adapt to insulin resistance. In our search for factors, with inhibitory effects on beta cells, we have recently described the inhibition of beta cell proliferation and insulin secretion by bone morphogenetic protein 4 (BMP4) [4].

BMPs belong to the Transforming Growth Factor-β (TGF-β) protein family, known to play central roles in pancreas and islet development [5-10]. While the role of BMPs in the developing pancreas and beta cell has gained much attention [8, 11, 12], less is known about their function in the postnatal pancreas. Increasing evidence indicates BMP2 and 4 to be inflammatory markers in various tissues under diabetic conditions [13-15]. We have recently shown that BMP2 and 4 are expressed in pancreatic islets, and are upregulated during diabetes progression in islets from *db/db* mice and by proinflammatory cytokines *in vitro* [4]. Although culture of pancreatic islets in the presence BMP2 and 4 negatively affects beta cell function, it appears that the effect of BMPs *in vivo* is more complex. Beta cell specific deletion of the BMP receptor 1A (BMPR1A) results in impaired glucose-induced insulin secretion (GSIS), whereas transgene BMP4 expression increase GSIS [16]. In contrast, deficiency of ID1, a central BMP regulated transcription factor, resulted in enhanced insulin secretion and protect from diet-induced glucose intolerance, suggesting that BMPs and ID1 normally exert inhibitory effects on adult beta cell function [17]. BMPs are released from and affect several metabolic relevant tissues, including fat, liver and kidney adding to the complexity of the role of BMPs in metabolism [14, 18, 19]. To characterize the direct effects of BMPs on beta cells we have recently reported BMP4

mediated inhibition of beta cell proliferation and repression of GSIS from mouse, rat and human islets [4]. Here, we further characterize the effects of BMP4 on insulin secretion by single cell electrophysiological measurements and evaluation of gene regulation to identify the molecular mechanism behind the observed inhibition of insulin secretion.

Research Design and Methods

Rat islet isolation and culture

Neonatal rat islets of Langerhans were isolated from 4-day-old Wistar rat pups (Taconic, Lille Skensved, Denmark) as previously described [20]. The isolated islets were pre-cultured for 7-10 days in RPMI 1640 with ultraglutamine (Lonza, Vallensbaek, Denmark) supplemented with 10% newborn calf serum (NCS) (Biological Industries, Kibbutz Beit Haemek, Israel), 100 U/ml penicillin and 100 µg/ml streptomycin (Gibco, Life Technologies, Taastrup, Denmark), in 5% CO_2 at 37°C. For experimental setups, rat islets cultured as intact and free-floating in medium supplemented with 2% human serum (Lonza (BioWhittaker) or as islets dispersed into single cells by 0.2% trypsin (Gibco), 10 mmol/L EDTA (Gibco) in HBSS. Dispersed islets were cultured on coverslips coated with bovine corneal extracellular matrix (ECM), (Biological Industries, Kibbutz Beit, Haemek, Israel) in the medium described above containing 2% human serum.

Mouse islet isolation and culture

Pancreatic islets from 10-12 weeks old female NMRI mice where isolated using collagenase digestions as previously described [21]. The islets were handpicked in albumin-coated Petri dishes (1 mg albumin/ml HBSS) and cultured for 1 day in medium I (RPMI 1640 with 10 mmol/L glucose and 10% fetal calf serum, 100 IU/ml penicillin, and 100 µg/ml streptomycin) and further 3 days in medium II (RPMI 1640 with 10 mM glucose and 2% fetal calf serum, 100 IU/ml penicillin, and 100 µg/ml streptomycin) in the

absence or presence of BMP4 (50 ng/ml). After culture, mouse islets were fixated for transmission electron microscopy (TEM) or dispersed into single cells, using Ca^{2+}-free buffer, for electrophysiological experiments.

Pancreatic islets from 12-19 week old 129SV/C57/6crl WT and Calbindin1 KO mice [22] were isolated by bileduct perfusion of the pancreas with liberase (Roche, Hvidovre, Denmark). Digestion was stopped by addition of HBSS buffer containing Mg^{2+} and Ca^{2+} (Gibco) and 3 g/L BSA and 0.5 g/L D-glucose. Islets were filtered through a 400 μm pore size mesh, followed by 100 μm and 70 μm mesh strainers (BD Falcon, Albertslund, Denmark). Retained islets were handpicked under a dissection microscope. Islets were cultured for 1 day in medium I. The following day islets were transferred to medium II, in which they were kept throughout stimulation. Female mice were used for electrophysiological experiments and male mice for insulin secretion assays.

Microarray analysis

800 intact, free-floating rat islets were cultured in 5.5 cm Sterilin dishes for 5-10 days and exposed to BMP4 for 96 hrs. Total RNA was extracted using TRIzol (Gibco). One microgram of total RNA was labelled by One-Cycle Target labeling kit (Affymetrix, Santa Clara, Ca, USA) following the instructions of the manufacturer. Hybridization cocktails were hybridised to Rat Genome 230 2.0 GeneChip® arrays (Affymetrix) at 45°C for 17 hours (60 RPM) in a Hybridization Oven 640 (Affymetrix). GeneChips® were washed and stained in a GeneChip® fluidics station 450 using the fluidics protocol "EukGE-WS2v5_450" (Affymetrix). Chips were scanned in a GeneChip® scanner 3000 (Affymetrix). Microarray data were normalized and gene expression measures derived using the RMA algorithm and the Bioconductor package "Affy" (http://www.bioconductor.org). Custom CDF (chip definition file) from brainarray.mbni.med.umich.edu was used. Qlucore Omics Explorer 3.0 (Qlucore AB, Sweden) was used for the statistical analysis of the normalized data. For

comparing BMP4 to vehicle treatment, the microarray data were variance filtered ($\sigma/\sigma(max)>0.1$), and the two groups compared (t-test, FDR=5% (Benjamini Hochberg correction for multiple testing)).

Analysis of Calbindin1 and Insulin1 mRNA expression by real-time qPCR

800 intact neonatal rat islets cultured for five days were exposed to 50 ng/ml BMP4 for the indicated time periods and total RNA extracted using TRIzol (LifeTechnologies). cDNA synthesis was performed by TaqMan Reverse Transcription Reagents (Applied Biosystems, CA, USA). TaqMan Gene Expression probes against rat *Calbindin1* (Rn00583140_m1), *Insulin 1* (Rn02121433_g1) and *Ppia* (Rn_00690933_m1) were from Applied Biosystems. The samples were run on ABI PRISM 7900 HT Taqman (Applied Biosystems). Each sample was run in duplicates or triplicates and expression was normalized to the internal control, *Ppia*.

Analysis of Calbindin1 protein expression by western blotting

1000 intact neonatal rat islets were cultured for 5-10 days prior to exposure to 50 ng/ml BMP4 for 24, 48, 72 or 96 hrs. SDS-PAGE and western blotting was performed as described previously [23]. Primary antibodies were rabbit anti-Calbindin1 (Cell Signaling Technology, AH Diagnostics, Aarhus, DK) and mouse-anti-β-actin (Abcam, Cambridge, UK). Chemiluminiscense was detected by Lumi-GLO (Cell Signaling Technology) and visualized by use of Las 3000 (Fuji Film). Densitometric scannings were performed in Image J (Freeware, NIH, Bethesda, Maryland, USA).

Glucose stimulated insulin secretion

7-10 days after isolation, forty neonatal rat islets were transferred to medium containing 2% human serum, 100 IU/ml penicillin, and 100 µg/ml streptomycin and stimulated with

50 ng/ml BMP4 for 0-96 hours. Mouse islets were stimulated the day after isolation. For each condition 20 islets were transferred to Krebs Ringer Hepes buffer (KRHB) (115 mmol/L NaCl, 4.7 mmol/L KCl,2.6 mmol/L $CaCl_2$, 1.2 mmol/L KH_2PO_4, 1.2 mmol/L $MgSO_4$, 10 mmol/L HEPES, 0.2% BSA, 2 mmol/L glutamine, 5 mmol/L $NaHCO_3$, 1% P/S, pH 7.4), Containing 2 mmol/L glucose and incubated for 90 minutes prior to the GSIS experiment. Islets were sequentially exposed to 2 mmol/L glucose, 20 mmol/L glucose and 20 mmol/L glucose plus 10µmol/L forskolin (Sigma-Aldrich, Brøndby, Denmark) for 30 minutes and buffer was collected from each condition. Insulin content was determined using an in-house insulin Elisa assay. Results were corrected for DNA content using Quant-IT™ PicoGreen ® dsDNA Reagent and Kit (Invitrogen, Life Technologies).

Production of Calbindin1 lenti virus

Mouse Calbindin1 cDNA in entry vector pENTR(tm) 221 (Invitrogen) was transferred to the pLenti6.2/v5DEST Gateway® Vector (Invitrogen). Lenti virus was produced in HEK293ft cells using the ViraPower™ Lenti viral Expression Systems (Invitrogen, Carlsbad, CA, USA) and lenti virus was harvested by ultra centrifugation. Titers were determined in HT1080 cells (Invitrogen). The virus was used at a MOI 5 for 6 hours.

Insulin release in single cells overexpressing Calbindin1 using lenti virus

Dispersed rat islet cells were cultured on coverslips coated with bovine corneal extracellular matrix (ECM) in 4 well containers for 4 days prior to transduction with Calbindin1 or GFP lenti virus for 6 hours at a MOI of 5. 96 hours after transduction, GSIS was evaluated as described above.

Electrophysiology

Capacitance measurements and ion-current measurements were performed on single beta cells in a mixture of dispersed islets cells using the patch-clamp technique as previously described [21]. Beta cells where identified by size and inactivation properties of the voltage dependent Na^+ channel [24, 25]. Exocytosis was evoked by a train of ten 500-ms depolarization from -70 mV to 0 mV with a frequency of 1Hz and measured as changes in membrane capacitance. The VDCC-currents to voltage relationship was determined by employing a protocol where the membrane was depolarized from -70 mV to between -40 mV to +40 mV for 50 ms.

Live calcium imaging

Islets were loaded with 4 μM Fura 2-AM (TefLabs) for 40 minutes followed by 30 minutes de-esterification in imaging buffer at pH 7.4 (mM: KCl 3.6, $MgSO_4$ 0.5, $CaCl_2$ 2.5, NaCl 140, $NaHCO_3$, NaH_2PO_3 0.5, HEPES 5). Imaging was performed with a Polychrome V monochromator (TILL Photonics, Graefeling, Germany) and a Nikon Eclipse Ti Microscope (Nikon, Tokyo, Japan) with a ER- BOB-100 trigger on an iXON3 camera and iQ2 (Andor Technology, Belfast, UK) software. Recording was performed at one frame per second at 37°C under perfusion 1ml/min. A region was marked around each islet and the light intensity was recoded in that region to get the integrated light intensity per unit area (μm^2) at 340nm (exposure 150 ms) and 380 nm (exposure 100 ms). These measured intensities were then used to calculate the ratio of Fura-2 bound (340 nm) and unbound (380 nm) to calcium at one frame per second.

Results:

BMP4 inhibits glucose stimulated insulin secretion

The effect of BMP4 on GSIS was investigated using neonatal rat islets. Pretreatment with 50 ng/ml BMP4 for 0-4 days resulted in a decrease in GSIS observed after 48 hours (Fig.

1a). Acute stimulation with BMP4 (0h) or pre-stimulation for up to 24 hours had no effect on insulin secretion. In addition doses as low as 2 ng/ml inhibits insulin secretion [4]. BMP4 stimulation had no effect on total islet insulin content (Fig. 1b) or *Ins1* mRNA levels (Fig. 1c). We did not observe any effect on the number, size or insulin granule proximity to the cell membrane using high resolution electron microscopy of adult mouse islets (Supplementary figure 1).

BMP4 inhibits exocytosis and voltage dependent Ca^{2+}-channel current

The fact that BMP4 inhibits GSIS without affecting total insulin content or total number of insulin granules, indicates that BMP4 may affect the secretory machinery. For further detailed electrophysiological analysis of insulin secretion we used dispersed primary mouse islet cells. We investigated exocytosis measured as an increase in membrane capacitance and found reduced depolarization-evoked increase in membrane capacitance in BMP4 treated primary mouse beta cells (Fig. 2a-e). The most pronounced effect was observed during the latter depolarizations (Depol 2-10; Fig 2d). This was further confirmed by a continued reduced exocytotic response to a second train of depolarizations performed 2 minutes later (Fig. 2e). Exocytosis is highly dependent on Ca^{2+}-influx through voltage-dependent Ca^{2+}-channels (VDCC) [26]. We therefore determined the VDCC-influx to voltage relationship (Fig. 2f-g). Beta cells exposed to BMP4 show ~50% reduced Ca^{2+}-influx at 0 mV. BMP4 increased the Ca^{2+}-sensitivity, i.e. the increase in membrane capacitance per Ca^{2+}-charge unit entering the cell, which suggests that the BMP4-dependent decrease in exocytosis is caused by a reduced Ca^{2+}-current rather than through a direct effect on exocytosis (Figure 2h). Moreover, BMP4 can be suggested to have a direct stimulatory effect on exocytosis that is less pronounced than the effect on the Ca^{2+}-current. To gain further insight into the mechanism on how BMP4 may cause reduced exocytosis we performed live calcium imaging in primary adult mouse islets. Evaluation of calcium

fluctuations was determined by differences in the Fura-2 340/380 ratio. Representative traces are shown in Figure 2i-j. All traces can be seen in supplementary Figure 1. Temporal fluctuation of intracellular calcium in response to glucose were organized into 2 classes: class 1 islets represent islets with separate 1st and 2nd phases with a clear 1st phase peak followed by a lowering of calcium and a 2nd phase with distinct regularly spaced calcium oscillations; class 2 islets present a rise in calcium with no clear first and second phases and no distinct oscillation in 2nd phase. In control islets we observed 64% and in BMP4 treated islets 26% to have a distinct 1st peak and 2nd phase oscillation in presence of high glucose (see Supplementary Table 1). In addition, there was a significant reduction in the first lowering of Ca^{2+} (Figure 2j and k) and the 1st phase peak amplitude at 16.7 mM glucose (Figure 2j and m) and the response to depolarizing K^+ (Figure 2j and o). The response time after increasing glucose concentrations was decreased by BMP4 treatment (Figure 2 j and l) whereas the response time to lowering of glucose was increased (Figure 2n). We did not observe significant changes in the amplitude or frequency of calcium oscillations.

BMP4 mediates upregulation of Calbindin1

Since the effects of BMP4 on GSIS are first observed after 48 hours exposure, we hypothesize that gene regulation is required for this effect. To unravel the mechanism of BMP4 mediated inhibition of GSIS we therefore performed a gene expression array comparing 3 independent set of vehicle and BMP4 (96h) treated neonatal rat islets. With a false discovery rate (FDR) of 5%, we find 102 genes to be regulated by BMP4 (Supplementary Table 2). The genes with more than 2-fold up- or downregulation are shown in Table 1. Seven of the gene regulations have been verified on independent rat islet samples (denoted with a * in Table 1).

We paid particular attention to genes known to be involved in hormone secretion and Ca^{2+}-handling based on the effects of BMP4 on insulin secretion, exocytosis and Ca^{2+}-channel

activity. We observed no regulation of the BMP receptors or L-type calcium channel subunits. One of the most regulated genes is Calbindin1, an EF-hand Ca^{2+}-binding protein which has previously been shown to regulate Ca^{2+}-currents through VDCC and inhibit GSIS in beta cells [27-29]. BMP4 increased the expression of Calbindin1 mRNA 6-fold in neonatal rat islets resulting in a 2.5 fold increase in Calbindin1 protein level after 96 hours (Figure 3a and b) As in primary neonatal rat islets, BMP4 increased the expression of Calbindin1 mRNA in adult mouse islets (Figure 3c).

Overexpression of Calbindin1 impairs GSIS

To determine the role of Calbindin1 in the BMP4 mediated effect on GSIS we induced overexpression of Calbindin1 in dispersed neonatal rat islet cells. Overexpression of Calbindin1 significantly reduced GSIS (Fig. 4a). Transfection efficiency was more than 80%, resulting in a robust upregulation of Calbindin1 protein (Fig. 4b).

BMP4 inhibition of GSIS and exocytosis is dependent on Calbindin1 upregulation

We further investigated the effect of BMP4 on GSIS from pancreatic islets isolated from Calbindin1 knock out (KO) mice and wild type (WT) littermates. Like in neonatal rat islets, we observed significant inhibition of GSIS by BMP4 treatment in WT adult mouse islets (Fig. 4c), whereas no inhibition was observed in islets from Calbindin KO mice (Fig. 4c). In accordance with this, we find that BMP4 does not reduce exocytosis in islets from Calbindin1 KO mice, but rather showed a non-significant increase in exocytosis (Fig. 4d-f).

Discussion:

Here we investigate the mechanism behind BMP4 mediated inhibition of GSIS in neonatal rat and adult mouse islets of Langerhans. This effect is not caused by decreased *Insulin1*

mRNA expression or protein content, or by number, size or localization of insulin granules, but rather seems to be due to diminished Ca^{2+}-influx through VDCC resulting in decreased exocytosis. Metabolism of glucose increase intracellular ATP levels resulting in closure of ATP dependent K^+ channels and membrane depolarization. Consequential opening of VDCC trigger Ca^{2+}-entry which elicits insulin exocytosis (reviewed in [30, 31]). Hence, Ca^{2+}-entry is essential for the amount of insulin released. We observe a BMP4 dependent decrease in VDCC Ca^{2+}-current leading to a reduction in depolarisation induced exocytosis and GSIS. Ca^{2+}-sensitivity of exocytosis was not decreased, rather increased, indicating that the reduced Ca^{2+} current is the main determinant of the reduced exocytosis. The reduced Ca^{2+}-influx was also confirmed by lack of response to K^+ in live Ca^{2+}-measurements. Both observations are indicative of reduced depolarization evoked Ca^{2+} -influx or increased Ca^{2+}-buffering after BMP4 treatment. An increased buffering would agree with the continued and more pronounced reduction in late exocytosis evoked by the latter depolarizations and the second train (Figure 2d-e). Interestingly, our microarray analysis identified the Ca^{2+}-binding protein Calbindin1 to be upregulated by BMP4. We refind this regulation on independent samples and in mouse islets. Although neonatal and adult islets have been suggested to respond different to glucose and other stimuli, BMP4 inhibit GSIS and upregulate Calbindin1 in both model systems. Overexpression of Calbindin1 reduced GSIS. The effect of BMP4 on GSIS was lost in islets from Calbindin1 KO mice (Fig. 4c). The exocytotic response to BMP4 in wild type islets showed the same trend as previously observed (Fig 4d and 2a-e), whereas this regulation was lost in islets from KO mice. There was a trend towards an increased exocytosis in response to BMP4 in the Calbindin1 KO mice, but this was not significant neither was it reflected in the GSIS. The observation that BMP induced inhibition of GSIS is not observed in islets from Calbindin1 KO mice points to the increased Calbindin1 expression being causative to the observed BMP4 mediated decline in GSIS. Indeed, the

BMP4 induced decrease in VDCC-influx is remarkably similar to the effect observed upon overexpression of Calbindin1 in a pancreatic beta cell line (Figure 2b-h and [29]). In addition to a Ca^{2+}-scavenging effect, accumulating evidence suggests that Calbindin1 reduce Ca^{2+}-currents through an association to L-type VDDCs [29]. A glucose and Ca^{2+} -dependent translocation of Calbindin1 to the plasma membrane has previously been suggested to facilitate the interaction with the L-type Ca^{2+}-channel [28, 29]. This could explain the lack of effect on the capacitance increase evoked by the first depolarisation (Figure 2c and 4e), as the first influx of Ca^{2+} would induce translocation of Calbindin1 to the plasma membrane.

Glucose induced Ca^{2+}-oscillations occur in fewer BMP4 treated islets compared to control cells possibly due to reduced Ca^{2+}-influx through VDCC. This is further supported by the blunted Ca^{2+} -response to high glucose and depolarizing K^+ after BMP4 treatment (Fig. 3i-o and Supplementary Table 1). The lack of K^+-induced Ca^{2+}-influx was also observed in a Calbindin1 overexpressing cell line, indicating that this is an effect caused by the increased Calbindin1 expression [27, 29]. Finally, the oscillations persist longer in BMP4 treated islets when glucose is lowered back to 2.8 mM (Figure 2n and Supplementary Table 1), indicating a failure of the beta cells to repolarize to baseline; again suggesting dysfunctional Ca^{2+} handling after BMP4 treatment.

Interestingly, Calbindin1 expression is increased in pancreatic islets from diabetic rats and mice [32, 33]. Concomitant upregulation of BMP2 (but not BMP4) and Calbindin1 in islets of Langerhans has been observed in a type 2 diabetic mouse model [33]. BMP2 also upregulate the expression of Calbindin1 and reduce GSIS in rat islets (data not shown). Generally BMP2 and 4 may be considered as inflammatory markers in several metabolic tissues. Under diabetic conditions the expression of BMP2 or 4 have been reported to increase in arteries, kidney, bones and islets [4, 14, 18, 19]. The increased expression is reflected by increased circulating levels of BMP4 in type 2 diabetic patients in one study

[13]. Thus, systemic inhibition of BMP2 and 4 appear as a possible strategy for broad targeting of a mediator of low grade inflammation associated with type 2 diabetes. Interestingly, it was recently reported that systemic administration of the natural BMP inhibitor noggin lowered blood glucose in *db/db* mice [14].

In conclusion, we have provided insight into mechanisms involved in BMP4 mediated inhibition of insulin secretion and gene regulation in islets of Langerhans and identified Calbindin1 as a mediator of BMP4 induced beta cell dysfunction.

Acknowledgements:

We acknowledge the technical assistance from Helle Fjordvang and Lene Grønne Pedersen, University of Copenhagen, Sabine Mach, Ludwig-Maximilians-Universität, Britt-Marie Nilsson and Anna-Maria Veljanovska-Ramsay, Lund University Diabetes Center.

Funding:

We are thankful for support from the Novo Nordisk Foundation, The Danish Research Council, The Danish Diabetes Academy, The European Foundation for the Study of Diabetes, The A.P. Møller Foundation, The Swedish Research Council, The Region Skåne (ALF), Albert Påhlsson foundation and The Swedish Diabetes foundation. LE is a senior Researcher at the Swedish Research Council. GLC hold a Postdoc grant from the Danish Diabetes Academy.

Dualty of interest:

MLBJ, CB and KSF are employees of Novo Nordisk A/S.

Contribution statement:

NB, GLC, MLBJ, CB and LE designed the study. GLC, MLBJ, AW, IM, JF, KSF, MM, CB, NB and LE participated in acquisition, analysis and interpretation of data. GLC, NB and LE

drafted the manuscript. GLC, MLBJ, AW, IM, JF, KSF, MM, CB, NB and LE revised the manuscript critically for important intellectual content and approved the final version to be published. NB is the guarantor of this work.

References:

[1] Weir GC, Bonner-Weir S (2004) Five stages of evolving beta-cell dysfunction during progression to diabetes. Diabetes 53 Suppl 3: S16-21

[2] Butler AE, Janson J, Bonner-Weir S, Ritzel R, Rizza RA, Butler PC (2003) Beta-cell deficit and increased beta-cell apoptosis in humans with type 2 diabetes. Diabetes 52: 102-110

[3] Rahier J, Guiot Y, Goebbels RM, Sempoux C, Henquin JC (2008) Pancreatic beta-cell mass in European subjects with type 2 diabetes. Diabetes, obesity & metabolism 10 Suppl 4: 32-42

[4] Bruun C, Christensen GL, Jacobsen ML, et al. (2014) Inhibition of beta cell growth and function by bone morphogenetic proteins. Diabetologia

[5] Sanvito F, Herrera PL, Huarte J, et al. (1994) TGF-beta 1 influences the relative development of the exocrine and endocrine pancreas in vitro. Development 120: 3451-3462

[6] Smart NG, Apelqvist AA, Gu X, et al. (2006) Conditional expression of Smad7 in pancreatic beta cells disrupts TGF-beta signaling and induces reversible diabetes mellitus. PLoS biology 4: e39

[7] Yamaoka T, Idehara C, Yano M, et al. (1998) Hypoplasia of pancreatic islets in transgenic mice expressing activin receptor mutants. The Journal of clinical investigation 102: 294-301

[8] Ahnfelt-Ronne J, Ravassard P, Pardanaud-Glavieux C, Scharfmann R, Serup P (2010) Mesenchymal bone morphogenetic protein signaling is required for normal pancreas development. Diabetes 59: 1948-1956

[9] Kumar M, Jordan N, Melton D, Grapin-Botton A (2003) Signals from lateral plate mesoderm instruct endoderm toward a pancreatic fate. Developmental biology 259: 109-122

[10] Sui L, Geens M, Sermon K, Bouwens L, Mfopou JK (2013) Role of BMP signaling in pancreatic progenitor differentiation from human embryonic stem cells. Stem cell reviews 9: 569-577

[11] Hogan BL (1996) Bone morphogenetic proteins in development. Current opinion in genetics & development 6: 432-438

[12] Little SC, Mullins MC (2006) Extracellular modulation of BMP activity in patterning the dorsoventral axis. Birth defects research Part C, Embryo today : reviews 78: 224-242

[13] Kim MK, Jang EH, Hong OK, et al. (2013) Changes in serum levels of bone morphogenic protein 4 and inflammatory cytokines after bariatric surgery in severely obese korean patients with type 2 diabetes. International journal of endocrinology 2013: 681205

[14] Koga M, Engberding N, Dikalova AE, et al. (2013) The bone morphogenic protein inhibitor, noggin, reduces glycemia and vascular inflammation in db/db mice. American journal of physiology Heart and circulatory physiology 305: H747-755

[15] Bostrom KI, Jumabay M, Matveyenko A, Nicholas SB, Yao Y (2011) Activation of vascular bone morphogenetic protein signaling in diabetes mellitus. Circulation research 108: 446-457

[16] Goulley J, Dahl U, Baeza N, Mishina Y, Edlund H (2007) BMP4-BMPR1A signaling in beta cells is required for and augments glucose-stimulated insulin secretion. Cell metabolism 5: 207-219

[17] Akerfeldt MC, Laybutt DR (2011) Inhibition of Id1 augments insulin secretion and protects against high-fat diet-induced glucose intolerance. Diabetes 60: 2506-2514
[18] Tominaga T, Abe H, Ueda O, et al. (2011) Activation of bone morphogenetic protein 4 signaling leads to glomerulosclerosis that mimics diabetic nephropathy. The Journal of biological chemistry 286: 20109-20116
[19] Koga M, Yamauchi A, Kanaoka Y, et al. (2013) BMP4 is increased in the aortas of diabetic ApoE knockout mice and enhances uptake of oxidized low density lipoprotein into peritoneal macrophages. Journal of inflammation 10: 32
[20] Brunstedt J (1980) Rapid isolation of functionally intact pancreatic islets from mice and rats by percollTM gradient centrifucation. Diabete & metabolisme 6: 87-89
[21] Eliasson L, Ma X, Renstrom E, et al. (2003) SUR1 regulates PKA-independent cAMP-induced granule priming in mouse pancreatic B-cells. The Journal of general physiology 121: 181-197
[22] Airaksinen MS, Eilers J, Garaschuk O, Thoenen H, Konnerth A, Meyer M (1997) Ataxia and altered dendritic calcium signaling in mice carrying a targeted null mutation of the calbindin D28k gene. Proceedings of the National Academy of Sciences of the United States of America 94: 1488-1493
[23] Frobose H, Ronn SG, Heding PE, et al. (2006) Suppressor of cytokine Signaling-3 inhibits interleukin-1 signaling by targeting the TRAF-6/TAK1 complex. Molecular endocrinology 20: 1587-1596
[24] Gopel S, Kanno T, Barg S, Galvanovskis J, Rorsman P (1999) Voltage-gated and resting membrane currents recorded from B-cells in intact mouse pancreatic islets. The Journal of physiology 521 Pt 3: 717-728
[25] Gopel SO, Kanno T, Barg S, Weng XG, Gromada J, Rorsman P (2000) Regulation of glucagon release in mouse -cells by KATP channels and inactivation of TTX-sensitive Na+ channels. The Journal of physiology 528: 509-520
[26] Ammala C, Eliasson L, Bokvist K, Larsson O, Ashcroft FM, Rorsman P (1993) Exocytosis elicited by action potentials and voltage-clamp calcium currents in individual mouse pancreatic B-cells. The Journal of physiology 472: 665-688
[27] Sooy K, Schermerhorn T, Noda M, et al. (1999) Calbindin-D(28k) controls [Ca(2+)](i) and insulin release. Evidence obtained from calbindin-d(28k) knockout mice and beta cell lines. The Journal of biological chemistry 274: 34343-34349
[28] Parkash J, Chaudhry MA, Amer AS, Christakos S, Rhoten WB (2002) Intracellular calcium ion response to glucose in beta-cells of calbindin-D28k nullmutant mice and in betaHC13 cells overexpressing calbindin-D28k. Endocrine 18: 221-229
[29] Lee D, Obukhov AG, Shen Q, et al. (2006) Calbindin-D28k decreases L-type calcium channel activity and modulates intracellular calcium homeostasis in response to K+ depolarization in a rat beta cell line RINr1046-38. Cell calcium 39: 475-485
[30] Rorsman P, Braun M (2013) Regulation of insulin secretion in human pancreatic islets. Annual review of physiology 75: 155-179
[31] Eliasson L, Abdulkader F, Braun M, Galvanovskis J, Hoppa MB, Rorsman P (2008) Novel aspects of the molecular mechanisms controlling insulin secretion. The Journal of physiology 586: 3313-3324
[32] Bazwinsky-Wutschke I, Wolgast S, Muhlbauer E, Peschke E (2010) Distribution patterns of calcium-binding proteins in pancreatic tissue of non-diabetic as well as type 2 diabetic rats and in rat insulinoma beta-cells (INS-1). Histochemistry and cell biology 134: 115-127
[33] Keller MP, Choi Y, Wang P, et al. (2008) A gene expression network model of type 2 diabetes links cell cycle regulation in islets with diabetes susceptibility. Genome research 18: 706-716

Figure legends.

Figure 1 BMP4 inhibits glucose stimulated insulin secretion without affecting total insulin content.

a) Neonatal rat islets were pre-exposed to 50 ng/ml BMP4 for 0-96 hours and GSIS was performed as described. b) Insulin content of islets post-assay. DNA content was used for normalization in a) and b). c) 8000 intact neonatal rat islets were exposed to 50 ng/ml BMP4 for 0-96 hours. *Ins1* mRNA expression is shown as relative values normalized against *Ppia* expression. All data are shown as mean +SEM. Statistical significance was evaluated using Anova followed by Dunnets t-test. * indicates $p<0.05$

Figure 2 BMP4 diminish capacitance and Ca^{2+} influx through voltage dependent Ca^{2+} channels

a) Example trace of depolarization-induced exocytosis, measured as changes in cell membrane capacitance (ΔC_m) in a single mouse beta cell. b) Mean increase in membrane capacitance evoked by a train of ten depolarizations, c) the first depolarization and d) depolarizations 2 to 10. e) Mean capacitance increase evoked by a second train applied 2 minutes later. f) Example trace from a VDCC in a beta cell incubated in the absence (grey) and presence of BMP4 (black). g) The measured charge (Q) as a function of the membrane voltage (V_m) during a 50 ms depolarization. Open squares; Ctrl cells, Black squares; BMP4 treated cells. h) The Ca^{2+}-sensitivity of the exocytotic response measured as the capacitance increase during the first depolarization of the train (ΔC_m) in c) divided by the Ca^{2+}-influx (Charge; Q) during the same 500 ms-depolarization. Data presented in b-e and g-h are mean ± SEM of n=9 to 16 experiments in each group. *$p<0.05$, **$p<0.01$. i) Representative example of a calcium trace obtained from one islet pre-treated for 3 days with vehicle (control) or j) BMP4. $\mathbf{C_0}$ - calcium dip occurring when 16.7 mM glucose reach the islets; $\mathbf{D_0}$ - time delay between 16.7 mM glucose exposure and the first calcium peak; $\mathbf{C_1}$ - amplitude of first phase peak; $\mathbf{D_1}$ - time delay in response to low glucose; $\mathbf{C_K}$ - amplitude of high potassium peak. The

staircase indicates the glucose concentration: 2.8 mmol/L glucose (2.8) and 16.7 mmol/L glucose (16.7). The line with K^+ indicate the addition of 70 mmol/L KCl. Summary statistics of calcium imaging traces shown in k) C_0, l) D_0, m)C_1, n) D_1 o) C_K

Figure 3 BMP4 stimulate the expression of Calbindin1

Islets were stimulated with 50 ng/ml BMP4 for 0-96 hours. a) Calbindin1 mRNA expression in neonatal rat islets is shown in relative values and normalized against the expression on *Ppia*. b) Protein expression in neonatal rat islets was determined by western blotting using primary antibodies against Calbindin1 and β-actin. A representative western blot is shown and quantification of densitometry of 3 blots was performed in image J. c) Isolated mouse islets were stimulated with 50 ng/ml BMP4 for 0-96 hours. *Calbindin1* mRNA expression is shown in relative amounts and normalized against the expression of *Ppia*. All data are presented as mean + SEM. n=3-4

Figure 4 Calbindin1 expression affects islet glucose and BMP4 responsiveness.

a) GSIS from dispersed neonatal rat islet cells overexpressing Calbindin1 or GFP. Insulin secretion is depicted as % of control cells exposed to high glucose. b) Western blot showing lentiviral overexpression of Calbindin1. c) Islets from Calbindin1 KO mice (KO) and littermate wild type controls (WT) were exposed to 50 ng/ml BMP4 for 96 hours and subsequently GSIS was determined, n=3. All data are presented as mean+SEM. d) Mean increase in membrane capacitance evoked by the full train, e) the first depolarization and f) 2-10th depolarizations in single mouse beta cells isolated from Calbindin1 KO mice (KO) and littermate wild type controls (WT).

Figure 1

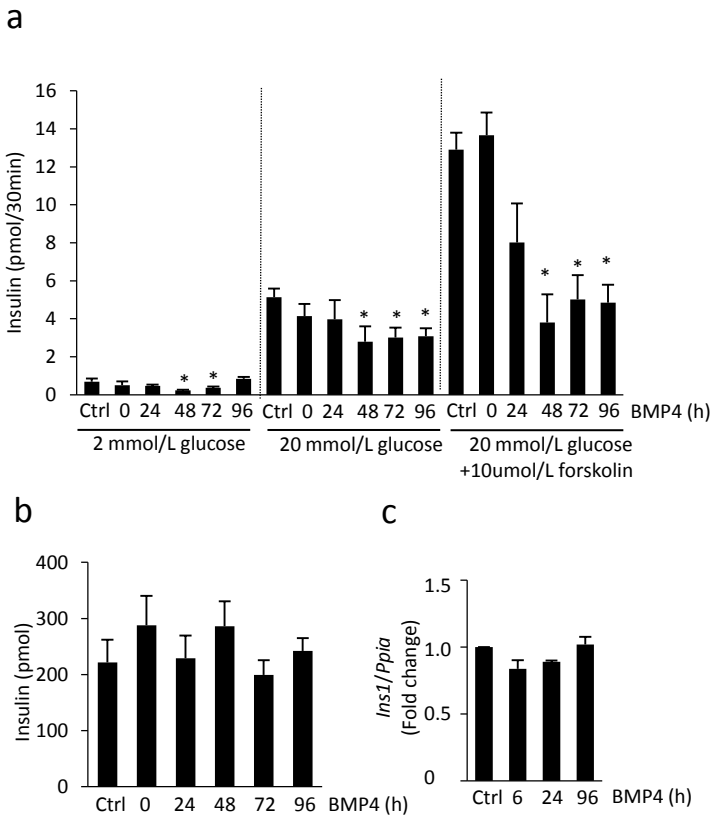
a
Insulin (pmol/30min)
16
14
12
10
8
6
4
2
0
Ctrl 0 24 48 72 96 Ctrl 0 24 48 72 96 Ctrl 0 24 48 72 96 BMP4 (h)
2 mmol/L glucose
20 mmol/L glucose
20 mmol/L glucose
+10umol/L forskolin
b
Insulin (pmol)
400
300
200
100
0
Ctrl 0 24 48 72 96 BMP4 (h)
c
Ins1/Ppia
(Fold change)
1.5
1.0
0.5
0
Ctrl 6 24 96 BMP4 (h)

Figure 2

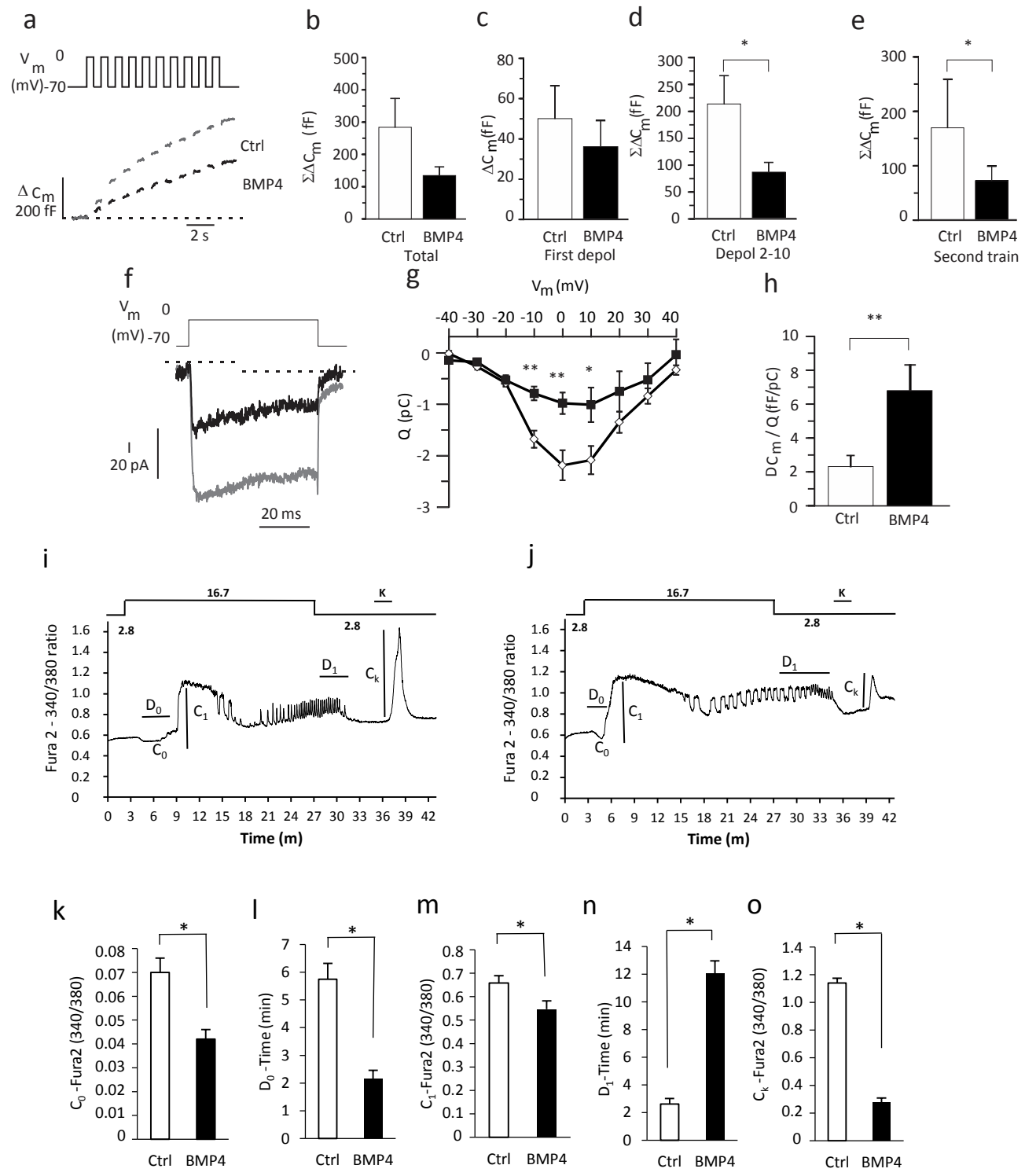
a
b
c
d
e
f
g
h
i
j
k
l
m
n
o
Ctrl
BMP4
2 s
Total
First depol
Depol 2-10
Second train
20 ms
Time (m)
16.7
K
2.8

Figure 3

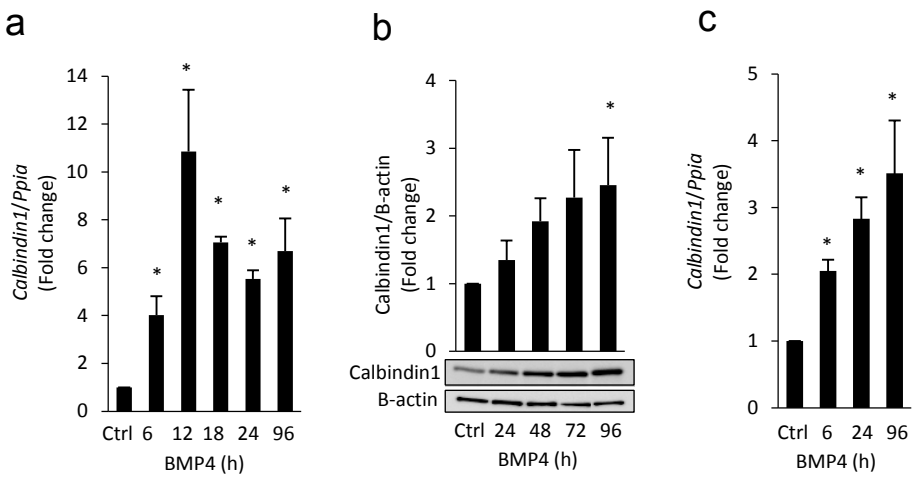
a
b
c
Calbindin1/Ppia
(Fold change)
Calbindin1/B-actin
(Fold change)
Calbindin1
B-actin
Ctrl 6 12 18 24 96
Ctrl 24 48 72 96
Ctrl 6 24 96
BMP4 (h)

Figure 4

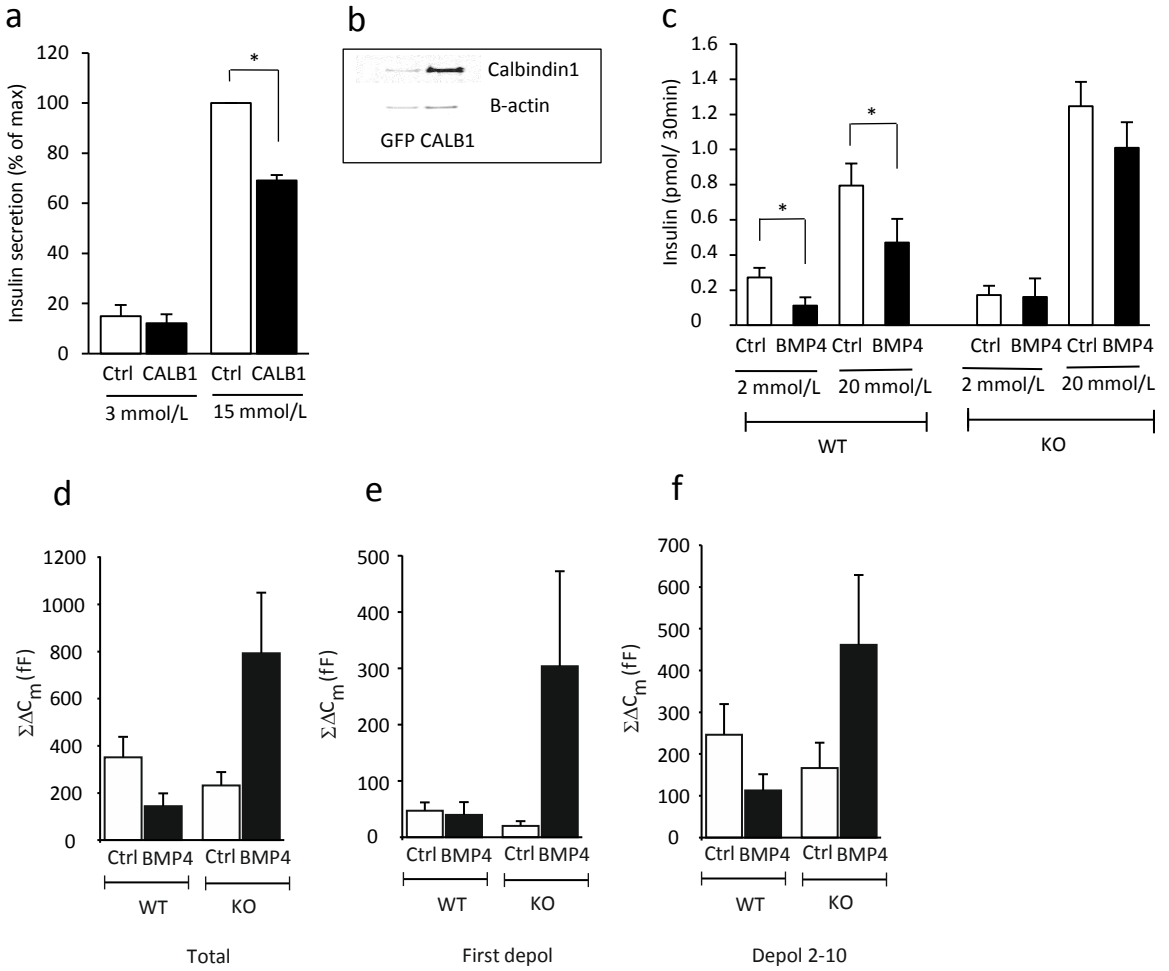
a
Insulin secretion (% of max)
120
100
80
60
40
20
0
*
Ctrl CALB1 Ctrl CALB1
3 mmol/L 15 mmol/L
b
Calbindin1
B-actin
GFP CALB1
c
Insulin (pmol/ 30min)
1.6
1.4
1.2
1.0
0.8
0.6
0.4
0.2
0
*
*
Ctrl BMP4 Ctrl BMP4 Ctrl BMP4 Ctrl BMP4
2 mmol/L 20 mmol/L 2 mmol/L 20 mmol/L
WT
KO
d
ΣΔCm (fF)
1200
1000
800
600
400
200
0
Ctrl BMP4 Ctrl BMP4
WT KO
Total
e
ΣΔCm (fF)
500
400
300
200
100
0
Ctrl BMP4 Ctrl BMP4
WT KO
First depol
f
ΣΔCm (fF)
700
600
500
400
300
200
100
0
Ctrl BMP4 Ctrl BMP4
WT KO
Depol 2-10

Table 1

Genes regulated ≥ 2-fold in neonatal rat islets exposed to 50 ng/ml BMP-4 for 96 hrs.

Gene	Protein name	Fold change
Id3	DNA-binding protein inhibitor ID-3	17.92*
Id1	DNA-binding protein inhibitor ID-1	16.52*
Lypd8	Ly6/PLAUR domain containing protein 8 precursor	9.66
Irx-3	Iroquois-class homeodomain protein IRX-3	5.40
Calb1	Calbindin1	4.62*
Id2	DNA-binding protein inhibitor ID-2	4.25*
Micalcl	MICAL C-terminal-like protein	4.06
Fam101a	Family with sequence similarity 101. member A (Fam101a)	3.85
Lgals4	Galectin-4	3.72
Bambi	BMP and activin membrane-bound inhibitor homolog	3.25*
Atoh8	Protein atonal homolog 8	3.13
Arc	Activity-regulated cytoskeleton-associated protein	3.08
Mlph	Melanophilin	2.90
Camk1g	Calcium/calmodulin-dependent protein kinase type 1G	2.82
Chst10	Carbohydrate sulfotransferase 10	2.81
Dlk1	Protein delta homolog 1	2.75
Tppp3	Tubulin polymerization-promoting protein family member 3	2.72
Tmem100	Transmembrane protein 100	2.68
Ckb	Creatine kinase B-type	2.63
Ppp1r36	Protein phosphatase 1 regulatory subunit 36	2.59
Tmem100	Transmembrane protein 100	2.51
Rtn4rl1	Reticulon-4 receptor-like 1	2.44
St5	Suppression of tumorigenicity 5 protein	2.34
Akap12	A-kinase anchor protein 12	2.30
Vash2	Vasohibin-2	2.20
Ddx31	Probable ATP-dependent RNA helicase DDX31	2.07
Fads1	Fatty acid desaturase 1	0.45
Nod3l	NOD3-like protein	0.44
Bmp3	Bone morphogenetic protein 3	0.43*
Htr5b	5-hydroxytryptamine (serotonin) receptor 5B	0.33
Gpr6	G protein-coupled receptor 6	0.28*

** Regulation have been verified by q-pcr on independent neonatal rat islet samples*

Supplementary Figure 1

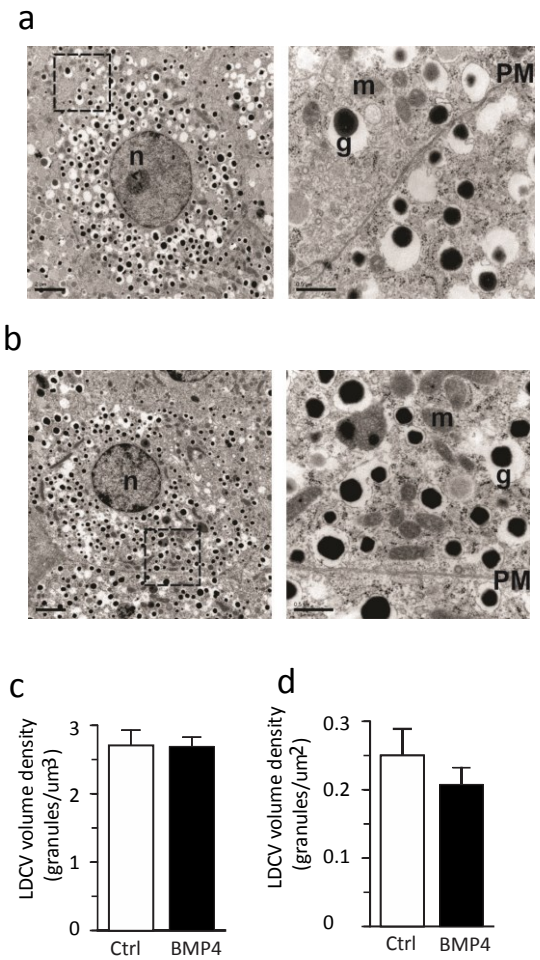

Supplementary figure 1
BMP4 does not affect the ultrastructure of mouse beta cells
a Transmission electron micrograph of a single beta cell within an islet that has been cultured in the absence of BMP4 (left; scale bar 2 µm). The area within the square is highlighted to the right (scale bar 0.5 µm). PM-plasma membrane; g-granule; m-mitochondria; n-nucleus. b As in a, but showing a single beta cell within an islet that have been cultured for 3 days in the presence of 50 ng/ml BMP4. C Histogram summarizing the total number of granules within beta cells after the different culture conditions presented as the volume density (granules/μm^3). d Histogram summarizing the number of docked granules within beta cells after the different culture conditions presented as the surface density (granules/μm^2). Granules were considered docked if the center of the granule was < 200 nm from the plasma membrane. Data in c and d is presented as mean + SEM of *n*= 30 (Ctrl) and 32 (BMP4) treated cells.

Method: Transmission electron microscopy
Mouse islets where fixed in 2.5% glutaraldehyde in freshly prepared Millonig and post-fixed in 1% osmium tetroxide before being dehydrated and embedded in AGAR 100 (Oxford Instruments Nordiska AB) and cut into ultrathin sections (70-90 nm). The sections were put on Cu-grids and contrasted using uranyl acetate and lead citrate. The islet containing sections were examined in a JEM 1230 electron microscope (JEOL-USA. Inc.). Micrographs were analysed with respect to the intracellular distribution as described elsewhere in as described elsewhere in Olofsson CS, et al 2002: Fast insulin secretion reflects exocytosis of docked granules in mouse pancreatic B-cells. Pflügers Arch 444:43-51”

Supplementary Figure 2

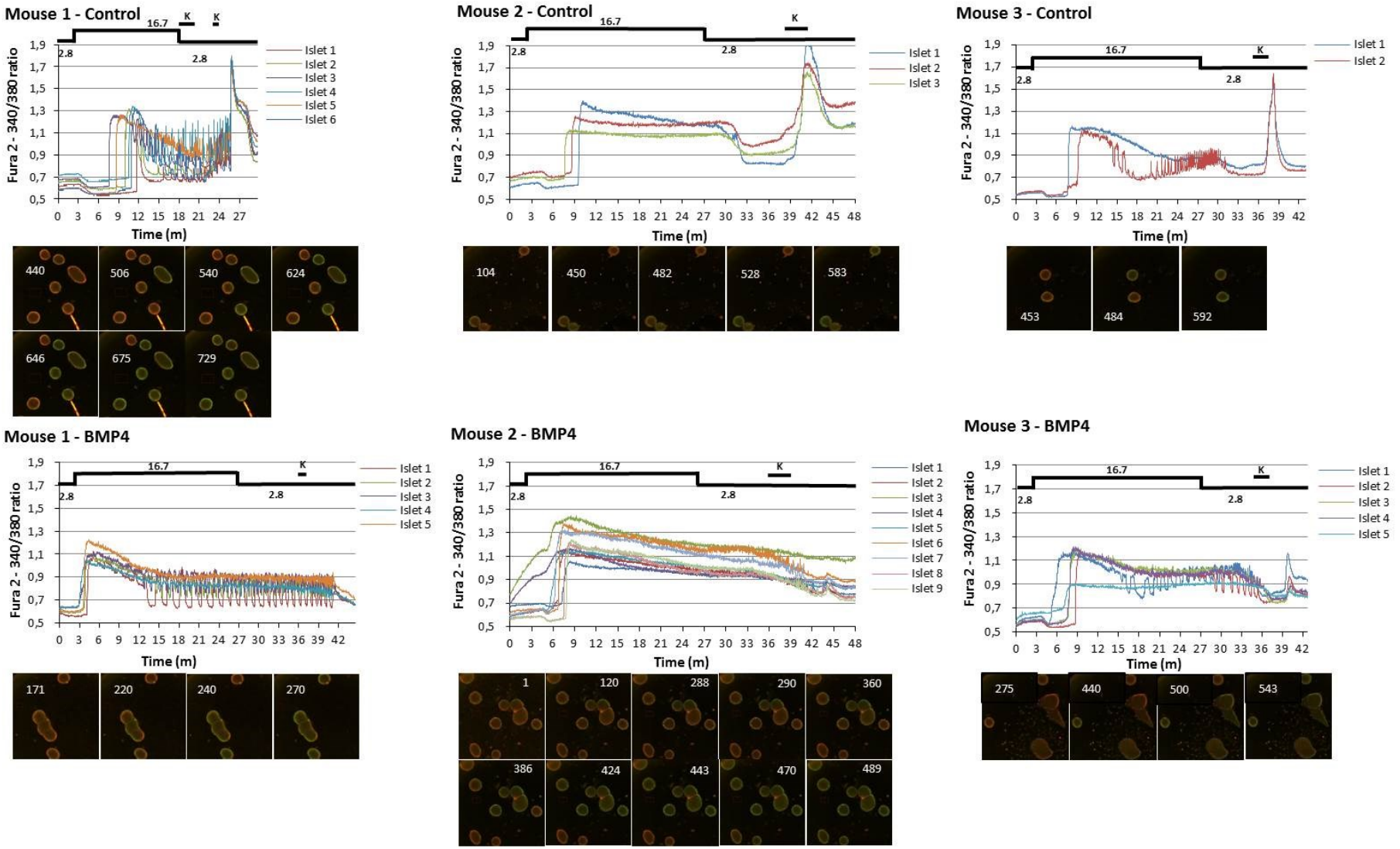

Figure 2

Traces of all islets imaged for each NMRI mouse under control or BMP4 conditioning. Below each trace are selected snapshots showing the relative position of the islets and the moment at which the first response to 16.7mM glucose can be visualized at 340nm (frame identified by number on image: 1 frame per second; 60 frames = 1 min). The position of each change in buffer perfusion: 2.8mM glucose (2.8), 16.7mM glucose (16.7), and 2.8mM glucose in 70mM KCl buffer (2.8 + K) are indicated by arrows above each set of traces.

Supplementary Table 1 – Summary statistics of calcium imaging traces

Parameter	C_0 (Fura2 340/380 ratio)						D_0 (min)						C_1 (Fura2 340/380 ratio)					
Islet Class	**All**		**Class 1**		**Class 2**		**All**		**Class 1**		**Class 2**		**All**		**Class 1**		**Class 2**	
Condition	**Ctrl**	**BMP4**	**Ctrl**	**BMP4**	**Ctrl**	**BMP4**	**Ctrl**	**BMP4**	**Ctrl**	**BMP4**	**Ctrl**	**BMP4**	**Ctrl**	**BMP4**	**Ctrl**	**BMP4**	**Ctrl**	**BMP4**
Number of islets	11	19	7	5	4	14	11	19	7	5	4	14	11	19	7	5	4	14
Mean	0.070	0.042	0.077	0.059	0.058	0.037	5.745	2.149	6.552	1.560	4.333	2.360	0.658	0.547	0.692	0.570	0.598	0.539
SEM	0.006	0.004	0.008	0.008	0.005	0.004	0.571	0.315	0.706	0.801	0.447	0.321	0.031	0.035	0.023	0.028	0.072	0.047
p-value	**5.63E-04**		0.15		**1.50E-02**		**1.78E-06**		**9.19E-04**		**8.05E-03**		**4.39E-02**		**7.04E-03**		0.56	

Parameter	F_H (peaks/min)		P_M (Fura2 340/380 ratio)						P_A (Fura2 340/380 ratio)			
Islet Class	**Class 1**		**All**		**Class 1**		**Class 2**		**Class 1**		**Class 2**	
Condition	**Ctrl**	**BMP4**	**Ctrl**	**BMP4**	**Ctrl**	**BMP4**	**Ctrl**	**BMP4**	**Ctrl**	**BMP4**	**Ctrl**	**BMP4**
Number of islets	7	5	11	19	7	5	4	14	7	5	4	14
Mean	1.357	0.940	0.962	0.997	0.884	0.892	1.100	1.035	0.168	0.126	0.030	0.031
SEM	0.248	0.234	0.046	0.029	0.032	0.033	0.079	0.033	0.019	0.027	0.002	0.002
p-value	0.27		0.51		0.87		0.39		0.22		0.84	

Parameter	D_1 (min) #						C_K (Fura2 340/380 ratio)					
Islet Class	**All**		**Class 1**		**Class 2**		**All**		**Class 1**		**Class 2**	
Condition	**Ctrl**	**BMP4**	**Ctrl**	**BMP4**	**Ctrl**	**BMP4**	**Ctrl**	**BMP4**	**Ctrl**	**BMP4**	**Ctrl**	**BMP4**
Number of islets	5	14	1	2	4	12	11	19	7	5	4	14
Mean	2.610	12.077	3.200	7.134	2.463	12.900	1.140	0.279	1.145	0.381	1.132	0.242
SEM	0.402	0.885	na	0.264	0.746	0.941	0.035	0.031	0.021	0.062	0.098	0.031
p-value	**6.02E-05**		na		**5.90E-05**		**8.03E-17**		**1.09E-07**		**2.97E-09**	

Supplementary Table 1 – Summary statistics of calcium imaging traces

Temporal fluctuation of intracellular calcium response to 16.7mM glucose were organized into 2 classes: class 1 islets present separate 1st and 2nd phases with a clear 1st phase peak followed by a lowering of calcium and a 2nd phase with distinct regularly spaced calcium oscillations; class 2 islets present a rise in calcium with no clear first and second phases and no distinct oscillation in 2nd phase. Evaluation of calcium fluctuations was made by measuring differences in Fura-2 340/380 ration points.

Calcium was measured in a total of 30 islets from 2-3 mice: 11control and 19 BPM4 treated islets. In control islets we observed 7/11 class islets (64%) and in BMP4 treated islets we observed 5/19 class 1 islets (26%). This reduction in the number of class 1 islets may represent a loss of first phase insulin secretion in the BMP4 treated islets.

$\mathbf{C_0}$ - calcium dip occurring when 16.7 mM glucose reach the islets and before 1st phase peak; $\mathbf{D_0}$ - time delay between the moment 16.7 mM glucose reached the islet and the first calcium peak; $\mathbf{C_1}$ - amplitude of first phase peak response to 16.7mM glucose; $\mathbf{F_H}$ - frequency of 2nd phase oscillations (in category 1 islets); $\mathbf{P_M}$ - mean ratio of oscillations during 2nd phase; $\mathbf{P_A}$ - mean amplitude of oscillations during 2nd phase; $\mathbf{D_1}$ - time delay in response to low glucose; $\mathbf{C_K}$ - amplitude of high potassium peak.

Supplementary table 2. Genes regulated by 96h treatment with 50 ng/ml BMP4 (FDR<5%)

id	gene	description	p-value	Fold change
ENSRNOG00000026124_at	Id3	DNA-binding protein inhibitor ID-3 [Source:UniProtKB/Swiss-Prot;Acc:P41138]	0,000114	17,92
ENSRNOG00000021750_at	Id1	DNA-binding protein inhibitor ID-1 [Source:UniProtKB/Swiss-Prot;Acc:P41135]	0,000025	16,52
ENSRNOG00000026844_at	LOC691259	RCG34567, isoform CRA_aUncharacterized protein [Source:UniProtKB/TrEMBL;Acc:D3ZP75]	0,003470	9,66
ENSRNOG00000011533_at	D3ZU03_RAT	iroquois-class homeodomain protein IRX-3 [Source:RefSeq peptide;Acc:NP_001100883]	0,000292	5,40
ENSRNOG00000007456_at	Calb1	Calbindin [Source:UniProtKB/Swiss-Prot;Acc:P07171]	0,000947	4,62
ENSRNOG00000007237_at	Id2	DNA-binding protein inhibitor ID-2 [Source:UniProtKB/Swiss-Prot;Acc:P41137]	0,000256	4,25
ENSRNOG00000016210_at	Micalcl	MICAL C-terminal-like protein [Source:UniProtKB/Swiss-Prot;Acc:Q4G091]	0,000225	4,06
ENSRNOG00000001011_at	Fam101a	family with sequence similarity 101, member A (Fam101a), mRNA [Source:RefSeq DNA;Acc:NM_001109547]	0,000003	3,85
ENSRNOG00000020338_at	Lgals4	Galectin-4 [Source:UniProtKB/Swiss-Prot;Acc:P38552]	0,003973	3,72
ENSRNOG00000016066_at	Bambi	BMP and activin membrane-bound inhibitor homolog [Source:UniProtKB/Swiss-Prot;Acc:Q91XN4]	0,000013	3,25
ENSRNOG00000010716_at	Atoh8	protein atonal homolog 8 [Source:RefSeq peptide;Acc:NP_001102711]	0,000457	3,13
ENSRNOG00000043465_at	Arc	Activity-regulated cytoskeleton-associated protein [Source:UniProtKB/Swiss-Prot;Acc:Q63053]	0,000800	3,08
ENSRNOG00000019763_at	Mlph	melanophilin [Source:RefSeq peptide;Acc:NP_001012135]	0,000037	2,90
ENSRNOG00000006470_at	Camk1g	Calcium/calmodulin-dependent protein kinase type 1G [Source:UniProtKB/Swiss-Prot;Acc:Q7TNJ7]	0,000093	2,82
ENSRNOG00000012815_at	Chst10	Carbohydrate sulfotransferase 10 [Source:UniProtKB/Swiss-Prot;Acc:O54702]	0,001042	2,81
ENSRNOG00000019584_at	Dlk1	protein delta homolog 1 [Source:RefSeq peptide;Acc:NP_446196]	0,003163	2,75
ENSRNOG00000016890_at	Tppp3	Tubulin polymerization-promoting protein family member 3 [Source:UniProtKB/Swiss-Prot;Acc:Q5PPN5]	0,000056	2,72
ENSRNOG00000038480_at	CN050_RAT	Uncharacterized protein C14orf50 homolog [Source:UniProtKB/Swiss-Prot;Acc:Q68FW6]	0,000013	2,68
ENSRNOG00000010872_at	Ckb	Creatine kinase B-type [Source:UniProtKB/Swiss-Prot;Acc:P07335]	0,000487	2,63
ENSRNOG00000001720_at	D4ADT9_RAT	Uncharacterized protein [Source:UniProtKB/TrEMBL;Acc:D4ADT9]	0,003472	2,59
ENSRNOG00000002434_at	Tmem100	Transmembrane protein 100 [Source:UniProtKB/Swiss-Prot;Acc:Q569C0]	0,002680	2,51
ENSRNOG00000003121_at	Rtn4rl1	Reticulon-4 receptor-like 1 [Source:UniProtKB/Swiss-Prot;Acc:Q80WD0]	0,001370	2,44
ENSRNOG00000013934_at	St5	suppression of tumorigenicity 5 protein [Source:RefSeq peptide;Acc:NP_001101017]	0,001590	2,34
ENSRNOG00000019549_at	Akap12	A-kinase anchor protein 12 [Source:UniProtKB/Swiss-Prot;Acc:Q5QD51]	0,000319	2,30
ENSRNOG00000003832_at	Vash2	vasohibin-2 [Source:RefSeq peptide;Acc:NP_001102552]	0,001632	2,20
ENSRNOG00000013040_at	Ddx31	probable ATP-dependent RNA helicase DDX31 [Source:RefSeq peptide;Acc:NP_001101294]	0,000066	2,07
ENSRNOG00000002209_at	D3Z8P4_RAT	arf-GAP with Rho-GAP domain, ANK repeat and PH domain-containing protein 2 [Source:RefSeq peptide;Acc:NP_001100686]	0,003196	2,00
ENSRNOG00000049873	Ap1s3	Adaptor-related protein complex 1, sigma 3 subunit	0,000577	1,97
ENSRNOG00000034075_at	Ube2ql1	ubiquitin-conjugating enzyme E2Q-like protein 1 [Source:RefSeq peptide;Acc:NP_001138635]	0,001700	1,97
ENSRNOG00000017873_at	Sct	Secretin [Source:UniProtKB/Swiss-Prot;Acc:P11384]	0,002561	1,95
ENSRNOG00000011824_at	Trh	ProthyroliberinThyroliberin [Source:UniProtKB/Swiss-Prot;Acc:P01150]	0,002298	1,93
ENSRNOG00000004828_at	Acvr1c	Activin receptor type-1C [Source:UniProtKB/Swiss-Prot;Acc:P70539]	0,003683	1,87
ENSRNOG00000001331_at	Rnf34	E3 ubiquitin-protein ligase RNF34 [Source:UniProtKB/Swiss-Prot;Acc:Q6AYH3]	0,000717	1,80
ENSRNOG00000004362_at	Rps6ka5	ribosomal protein S6 kinase alpha-5 [Source:RefSeq peptide;Acc:NP_001101518]	0,000179	1,74
ENSRNOG00000022704	Esyt3	Extended synaptotagmin-like protein 3	0,003161	1,73
ENSRNOG00000036693_at	Slc25a10	mitochondrial dicarboxylate carrier [Source:RefSeq peptide;Acc:NP_596909]	0,000314	1,67
ENSRNOG00000009761_at	Tmod1	Tropomodulin-1 [Source:UniProtKB/Swiss-Prot;Acc:P70567]	0,003524	1,64
ENSRNOG00000027888_at	RGD1309437	Uncharacterized protein C3orf26 homolog [Source:UniProtKB/Swiss-Prot;Acc:Q5FVR6]	0,001291	1,62
ENSRNOG00000002191_at	LOC498368	Uncharacterized protein C4orf19 homolog [Source:UniProtKB/Swiss-Prot;Acc:Q6AYA8]	0,003808	1,62
ENSRNOG00000006519_at	Tmem107	transmembrane protein 107 [Source:RefSeq peptide;Acc:NP_001103118]	0,002142	1,62
ENSRNOG00000036816_at	WLS_RAT	protein wntless homolog isoform 1 [Source:RefSeq peptide;Acc:NP_955440]	0,001280	1,61
ENSRNOG00000038686_at	Ap1s2	AP-1 complex subunit sigma-2 [Source:RefSeq peptide;Acc:NP_001121003]	0,000012	1,59
ENSRNOG00000012513_at	Pdk3	pyruvate dehydrogenase kinase, isozyme 3 [Source:RefSeq peptide;Acc:NP_001100051]	0,001113	1,56
ENSRNOG00000019466_at	Agpat2	1-acyl-sn-glycerol-3-phosphate acyltransferase beta [Source:RefSeq peptide;Acc:NP_001101291]	0,000605	1,56
ENSRNOG00000012787_at	Tmem164	transmembrane protein 164 [Source:RefSeq peptide;Acc:NP_001102484]	0,000684	1,55
ENSRNOG00000018106_at	Neu3	Sialidase-3 [Source:UniProtKB/Swiss-Prot;Acc:Q99PW5]	0,000168	1,55
ENSRNOG00000013286_at	Pdcl3	Phosducin-like protein 3 [Source:UniProtKB/Swiss-Prot;Acc:Q4KLJ8]	0,004009	1,52
ENSRNOG00000036692_at	Gcgr	Glucagon receptor [Source:UniProtKB/Swiss-Prot;Acc:P30082]	0,002636	1,50
ENSRNOG00000004200_at	Golsyn	Uncharacterized protein [Source:UniProtKB/TrEMBL;Acc:F1LUC0]	0,000378	1,50
ENSRNOG00000049019	Tmem170a	Transmembrane protein 170A	0,001936	1,49
ENSRNOG00000007023_at	Galm	Aldose 1-epimerase [Source:UniProtKB/Swiss-Prot;Acc:Q66HG4]	0,001670	1,49
ENSRNOG00000018359_at	Smad7	Mothers against decapentaplegic homolog 7 [Source:UniProtKB/Swiss-Prot;Acc:O88406]	0,000303	1,47
ENSRNOG00000001958_at	Ift57	intraflagellar transport protein 57 homolog [Source:RefSeq peptide;Acc:NP_001100563]	0,001778	1,46
ENSRNOG00000020939_at	Ms4a8a	membrane-spanning 4-domains, subfamily A, member 8A [Source:RefSeq peptide;Acc:NP_001101989]	0,000367	1,45
ENSRNOG00000002866_at	Rassf6	Ras association domain-containing protein 6 [Source:UniProtKB/Swiss-Prot;Acc:Q4QR82]	0,002048	1,44
ENSRNOG00000012597_at	RGD1311805	similar to RIKEN cDNA 2400010D15 (RGD1311805), mRNA [Source:RefSeq DNA;Acc:NM_001009638]	0,000061	1,41
ENSRNOG00000019346_at	Tmco3	transmembrane and coiled-coil domain-containing protein 3 [Source:RefSeq peptide;Acc:NP_001129329]	0,000804	1,41
ENSRNOG00000001090_at	Stard13	stAR-related lipid transfer protein 13 [Source:RefSeq peptide;Acc:NP_001102530]	0,004083	1,41
ENSRNOG00000016558_at	Pllp	Plasmolipin [Source:UniProtKB/Swiss-Prot;Acc:P47987]	0,001675	1,39
ENSRNOG00000013557_at	Lancl1	LanC-like protein 1 [Source:UniProtKB/Swiss-Prot;Acc:Q9QX69]	0,002269	1,38
ENSRNOG00000006302_at	Gclc	Glutamate--cysteine ligase catalytic subunit [Source:UniProtKB/Swiss-Prot;Acc:P19468]	0,000674	1,37
ENSRNOG00000009892_at	Adamts15	A disintegrin and metalloproteinase with thrombospondin motifs 15 [Source:RefSeq peptide;Acc:NP_001100280]	0,001249	1,37
ENSRNOG00000016338_at	Fam92a1	Uncharacterized protein [Source:UniProtKB/TrEMBL;Acc:D3ZP87]	0,000627	0,73
ENSRNOG00000028640_at	Siva1	Apoptosis regulatory protein Siva [Source:UniProtKB/Swiss-Prot;Acc:P59692]	0,001121	0,72
ENSRNOG00000027767_at	Slc38a5	Sodium-coupled neutral amino acid transporter 5 [Source:UniProtKB/Swiss-Prot;Acc:A2VCW5]	0,002558	0,71
ENSRNOG00000009372_at	Tacr3	Neuromedin-K receptor [Source:UniProtKB/Swiss-Prot;Acc:P16177]	0,000105	0,71
ENSRNOG00000009779_at	Krt8	Keratin, type II cytoskeletal 8 [Source:UniProtKB/Swiss-Prot;Acc:Q10758]	0,002497	0,71
ENSRNOG00000002095_at	Arhgap24	Rho GTPase-activating protein 24 [Source:UniProtKB/Swiss-Prot;Acc:Q5U2Z7]	0,000905	0,71
ENSRNOG00000006200_at	St18	Suppression of tumorigenicity 18 protein [Source:UniProtKB/Swiss-Prot;Acc:Q9QX27]	0,000132	0,71
ENSRNOG00000014549	Arhgef26	Rho gianine nucleotide exchange factor (GEF) 26	0,002788	0,71
ENSRNOG00000020456_at	Nucb2	Nucleobindin-2 [Source:UniProtKB/Swiss-Prot;Acc:Q9JI85]	0,002516	0,70
ENSRNOG00000005589_at	RGD1565002	Uncharacterized protein [Source:UniProtKB/TrEMBL;Acc:D4A0T8]	0,000693	0,70
ENSRNOG00000017209_at	Tubb3	Tubulin beta-3 chain [Source:UniProtKB/Swiss-Prot;Acc:Q4QRB4]	0,003566	0,69
ENSRNOG00000003915_at	Tmem206	Transmembrane protein 206 [Source:UniProtKB/Swiss-Prot;Acc:Q66H28]	0,000320	0,69
ENSRNOG00000000606_at	Pcdh15	Uncharacterized protein [Source:UniProtKB/TrEMBL;Acc:F1LT00]	0,002055	0,68
ENSRNOG00000021870_at	Slco4a1	Solute carrier organic anion transporter family member 4A1 [Source:UniProtKB/Swiss-Prot;Acc:Q99N01]	0,000636	0,68
ENSRNOG00000011421_at	Smap2	stromal membrane-associated GTPase-activating protein 2 [Source:RefSeq peptide;Acc:NP_001094139]	0,003692	0,68
ENSRNOG00000017965_at	Afg3l2	AFG3-like protein 2 [Source:RefSeq peptide;Acc:NP_001128336]	0,001111	0,68
ENSRNOG00000007808_at	Nap1l5	Nucleosome assembly protein 1-like 5 [Source:UniProtKB/Swiss-Prot;Acc:Q5PPG6]	0,000447	0,68
ENSRNOG00000008526_at	Pdzd3	Na(+)/H(+) exchange regulatory cofactor NHE-RF4 [Source:RefSeq peptide;Acc:NP_001178925]	0,000112	0,67
ENSRNOG00000016827_at	Slc38a3	Sodium-coupled neutral amino acid transporter 3 [Source:UniProtKB/Swiss-Prot;Acc:Q9JHZ9]	0,002477	0,67
ENSRNOG00000019587_at	Ptprn	Receptor-type tyrosine-protein phosphatase-like N [Source:UniProtKB/Swiss-Prot;Acc:Q63259]	0,000613	0,66
ENSRNOG00000002151_at	TAGL3_RAT	Transgelin-3 [Source:UniProtKB/Swiss-Prot;Acc:P37805]	0,002394	0,66
ENSRNOG00000013215_at	DCTD_RAT	Deoxycytidylate deaminase [Source:UniProtKB/Swiss-Prot;Acc:Q5M9G0]	0,000715	0,63
ENSRNOG00000001628_at	Pcp4	Purkinje cell protein 4 [Source:UniProtKB/Swiss-Prot;Acc:P63055]	0,000133	0,63
ENSRNOG00000010753_at	Aig1	androgen-induced gene 1 protein [Source:RefSeq peptide;Acc:NP_001127897]	0,000486	0,63
ENSRNOG00000002579_at	Parm1	Prostate androgen-regulated mucin-like protein 1 homolog [Source:UniProtKB/Swiss-Prot;Acc:Q6P9X9]	0,000667	0,62
ENSRNOG00000012183_at	Glrx1	Glutaredoxin-1 [Source:UniProtKB/Swiss-Prot;Acc:Q9ESH6]	0,000256	0,61
ENSRNOG00000014819_at	Hap1	Huntingtin-associated protein 1 [Source:UniProtKB/Swiss-Prot;Acc:P54256]	0,000601	0,60
ENSRNOG00000024923_at	Nnat	Neuronatin [Source:UniProtKB/Swiss-Prot;Acc:Q62649]	0,000459	0,60
ENSRNOG00000020455_at	Cst6	cystatin-M [Source:RefSeq peptide;Acc:NP_598250]	0,000069	0,58
ENSRNOG00000032669_at	Serpina1	Alpha-1-antiproteinase [Source:UniProtKB/Swiss-Prot;Acc:P17475]	0,001816	0,56
ENSRNOG00000007600_at	Igsf1	Immunoglobulin superfamily member 1 [Source:UniProtKB/Swiss-Prot;Acc:Q925N6]	0,000485	0,54
ENSRNOG00000011201_at	Cmtm8	CKLF-like MARVEL transmembrane domain-containing protein 8 [Source:RefSeq peptide;Acc:NP_942049]	0,000689	0,54
ENSRNOG00000014264_at	Phactr1	Phosphatase and actin regulator 1 [Source:UniProtKB/Swiss-Prot;Acc:P62024]	0,003136	0,52
ENSRNOG00000005615_at	Gadd45a	Growth arrest and DNA damage-inducible protein GADD45 alpha [Source:UniProtKB/Swiss-Prot;Acc:P48317]	0,000084	0,51
ENSRNOG00000015971_at	Slc12a2	solute carrier family 12 member 2 [Source:RefSeq peptide;Acc:NP_113986]	0,003419	0,50
ENSRNOG00000020480_at	Fads1	Fatty acid desaturase 1 [Source:UniProtKB/Swiss-Prot;Acc:Q920R3]	0,001893	0,45
ENSRNOG00000039856_at	nod3l	Uncharacterized protein C6orf154 homolog [Source:UniProtKB/Swiss-Prot;Acc:Q587K4]	0,002516	0,44
ENSRNOG00000002381_at	Bmp3	Bone morphogenetic protein 3 [Source:UniProtKB/Swiss-Prot;Acc:P49002]	0,002547	0,43
ENSRNOG00000002549	HTR5B	5-hydroxytryptamine (serotonin) receptor 5B	0,003570	0,33
ENSRNOG00000049580	GPR6	G protein-coupled receptor 6	0,000178	0,29